Intrazeolite Phototopotaxy: EXAFS Analysis of Precursor 8{W(CO)$_6$}-Na$_{56}$Y and Photooxidation Products 16(WO$_3$)-Na$_{56}$Y and 28(WO$_3$)-Na$_{56}$Y

Karin Moller,* Thomas Bein,

Department of Chemistry, University of New Mexico, Albuquerque, New Mexico 87131

Saim Özkar,† and Geoffrey A. Ozin*

Lash Miller Chemistry Department, University of Toronto, Toronto, Ontario, Canada M5S 1A1
(Received: November 26, 1990)

The intrazeolite photooxidation chemistry of α-cage encapsulated hexacarbonyltungsten(0) in Na$_{56}$Y with O$_2$, denoted n{W(CO)$_6$}-Na$_{56}$Y/O$_2$/$h\nu$, which has previously been shown to provide a novel synthetic pathway to α-cage located tungsten(VI) oxide, denoted n(WO$_3$)-Na$_{56}$Y, is now the subject of an extended X-ray absorption fine structure (EXAFS) analysis. The EXAFS data of a precursor 8{W(CO)$_6$}-Na$_{56}$Y, which contains on average one W(CO)$_6$ per α-cage shows that the W(CO)$_6$ guest maintains its structural integrity with only minor observable perturbations of the skeletal WC and ligand CO bonds compared to those found for the same molecule in the free state. The EXAFS analysis results for the photooxidation products 16(WO$_3$)-Na$_{56}$Y and 28(WO$_3$)-Na$_{56}$Y are very similar and display the presence of two terminal tungsten-oxygen bonds (1.75-1.77 Å) and two bridging tungsten-oxide bonds (1.94-1.95 Å), together with a short distance to a second tungsten (3.24-3.30 Å). This bond length and coordination number information for n = 16 and 28 samples is best interpreted in terms of the formation of a single kind of tungsten trioxide dimer unit (WO$_3$)$_2$, most likely interacting with extraframework Na$^+$ cations, denoted ZONa···O$_2$W(μ-O)$_2$WO$_2$···NaOZ. In conjunction with earlier chemical and spectroscopic information on this system, the EXAFS data support the contention that 16(WO$_3$)-Na$_{56}$Y contains a uniform array of single size and shape tungsten(VI) oxide dimers (WO$_3$)$_2$ housed in the 13-Å supercages of the zeolite Y host. The sequential addition of WO$_3$ units to the 16(WO$_3$)-Na$_{56}$Y sample appears to increase the (WO$_3$)$_2$ dimer population, causing a buildup of α-cage encapsulated dimers-of-dimers {(WO$_3$)$_2$}$_2$ rather than further cluster growth to trimers (WO$_3$)$_2$ and/or tetramers (WO$_3$)$_4$.

Introduction

Metal organic chemical vapor deposition (MOCVD) has proven to have enormous technological importance in the epitaxial and photoepitaxial production of thin films and low dimensional quantum nanostructures for use in electronic and optical devices.[1] Thermal MOCVD has only very recently been used for the synthesis of intrazeolite quantum supralattices[2] which are of great current interest for future applications in quantum electronic and nonlinear optical devices.[3]

We recently demonstrated[4] that the photooxidation of α-cage encapsulated hexacarbonyltungsten(0), n{W(CO)$_6$}-Na$_{56}$Y, provides a mild, clean, and quantitative synthetic pathway to α-cage encapsulated, single-size tungsten(VI) oxide clusters n(WO$_3$)-Na$_{56}$Y according to the reaction scheme

$$n\{W(CO)_6\}\text{-}Na_{56}Y + \tfrac{9}{2}nO_2 \xrightarrow{h\nu} n(WO_3)\text{-}Na_{56}Y + 6nCO_2$$

We like to refer to this kind of three-dimensional surface, host-guest inclusion chemistry as "intrazeolite metal carbonyl phototopotaxy" to bring forth the resemblance to a similar type of photochemistry performed on a two-dimensional surface known as photoepitaxy.[5]

This type of intrazeolite W(CO)$_6$ photooxidation chemistry was anticipated to proceed cleanly to zeolite Y encapsulated WO$_3$ aggregates, based on precedents in the organometallic and matrix isolation literature exemplified by the following rhenium(I)[6] and molybdenum(0)[7] systems:

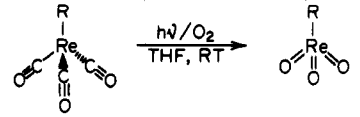

(R = CH$_3$, C$_5$H$_5$)

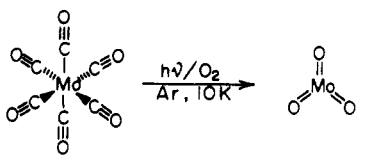

†On sabbatical leave from the Chemistry Department, Middle East Technical University, Ankara, Turkey.

In the case of the precursor n{W(CO)$_6$}-Na$_{56}$Y, the key points that have emerged from the chemical and spectroscopic studies[4,8] include the following: (i) the hexacarbonyltungsten(0) molecule appears to be associated with two α-cage extraframework Na$^+$ cations (or Brønsted protons for H$_{56}$Y as host), via the oxygen end of two trans-bonded carbonyl ligands with saturation loading of two W(CO)$_6$ per α-cage; (ii) the hexacarbonyltungsten(0) guest is confined to the internal surface of the zeolite Y host with a homogeneous distribution throughout the zeolite crystals.

With respect to the product n(WO$_3$)-Na$_{56}$Y, it has been discovered[4] that a sequential saturation loading/photooxidation scheme of the type laid out below satisfactorily accounts for the chemistry and spectroscopy of the system:

$$16W(CO)_6\text{-}Na_{56}Y(H_{56}Y) \longrightarrow 16WO_3\text{-}Na_{56}Y(H_{56}Y) \longrightarrow$$
$$8W(CO)_6,\ 16WO_3\text{-}Na_{56}Y(H_{56}Y) \longrightarrow 24WO_3\text{-}Na_{56}Y(H_{56}Y) \longrightarrow$$
$$4W(CO)_6,\ 24WO_3\text{-}Na_{56}Y(H_{56}Y) \longrightarrow 28WO_3\text{-}Na_{56}Y(H_{56}Y) \longrightarrow$$
$$\vdots \qquad\qquad \vdots$$
$$0.1W(CO)_6,\ 31.9WO_3\text{-}Na_{56}Y(H_{56}Y) \longrightarrow 32WO_3\text{-}Na_{56}Y(H_{56}Y)$$

By employing the above impregnation method, it proved possible to organize the intrazeolite tungsten(VI) oxide system from one containing what was believed at the time to be isolated (uncoupled) α-cage encapsulated (WO$_3$)$_2$ dimers at n < 8, to a quantum

(1) Ploog, K. *Angew. Chem., Int. Ed. Engl.* **1988**, *27*, 593; *Nanostructure Physics and Fabrication*; Reed, M. A., Kirk, W. P., Eds.; Academic Press: New York, 1988 and references cited therein.
(2) Ozin, G. A.; Kuperman, A.; Stein, A. *Angew. Chem.* **1989**, *101*, 373. Stucky, G. D.; MacDougall, J. E. *Science* **1990**, *247*, 669 and references cited therein.
(3) Miller, D. A. B.; Schmitt-Rink, S.; Chemla, D. S. *Phys. Rev. B* **1987**, *35*, 8113 and references cited therein.
(4) Ozin, G. A.; Özkar, S. *J. Phys. Chem.* **1990**, *94*, 7556.
(5) Almond, M. J.; Rice, D. A.; Yates, C. A. *Chem. Br.* **1988**, *24*, 1130 and references cited therein.
(6) Hermann, W. A. *J. Organomet. Chem.* **1986**, *300*, 111; *Angew. Chem., Int. Ed. Engl.* **1988**, *27*, 1297.
(7) Almond, M. J.; Crayston, J. A.; Downs, A. J.; Poliakoff, M.; Turner, J. *Inorg. Chem.* **1986**, *25*, 19 and references cited therein.
(8) Özkar, S.; Ozin, G. A.; Moller, K.; Bein, T. *J. Am. Chem. Soc.* **1990**, *112*, 9575.

0022-3654/91/2095-5276$02.50/0

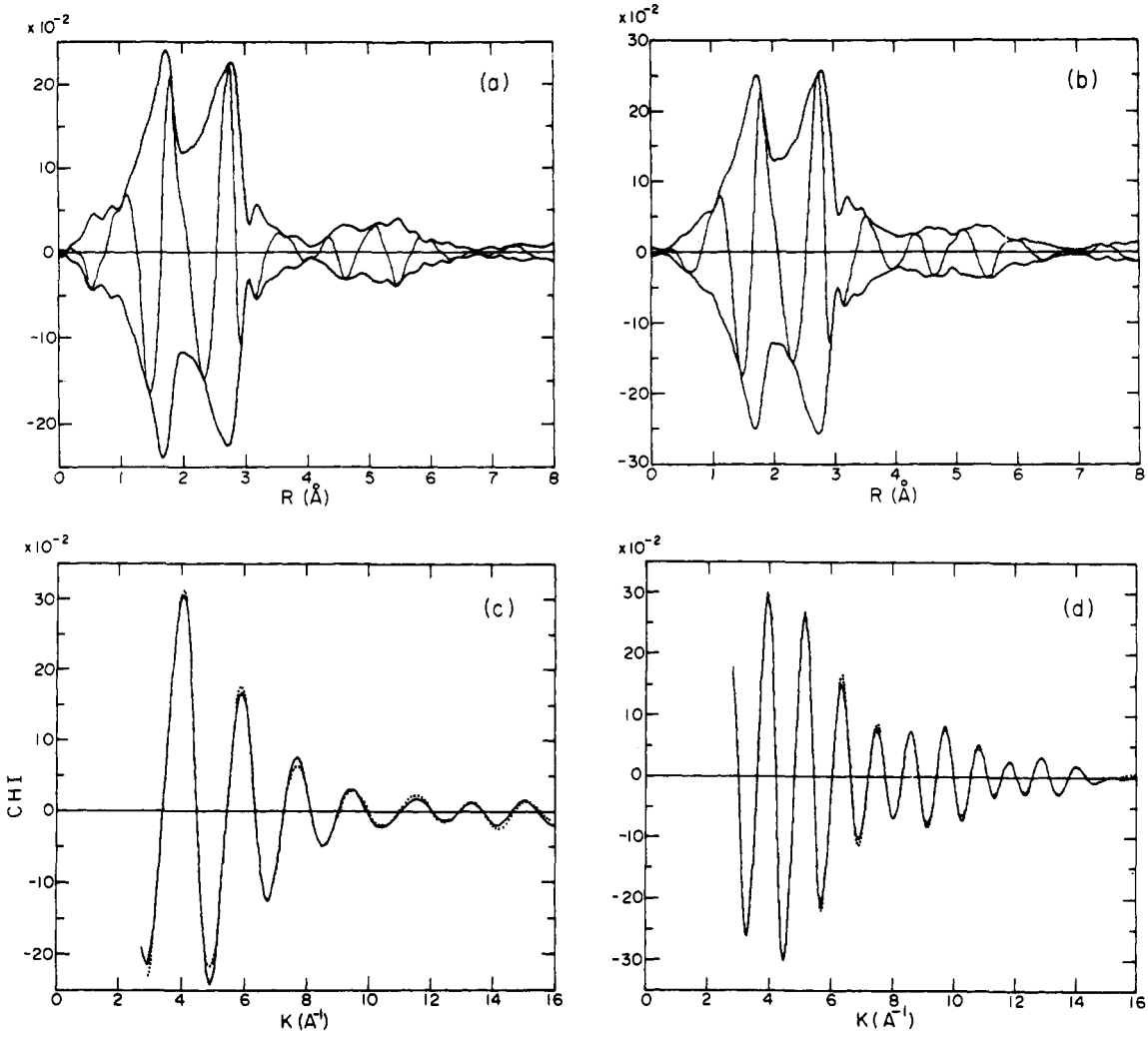

Figure 1. k^1-weighed Fourier transformation (k = 3–16 Å^{-1}) of (a) $W(CO)_6$ reference and (b) sample $8\{W(CO)_6\}$–$Na_{56}Y$. (b and c) Back-transformations of (c) first shell (0–2.0 Å) and (d) second shell (2.0–3.3 Å) of sample $8\{W(CO)_6\}$–$Na_{56}Y$; original data (solid line) and fit (broken line).

supralattice built of coupled $(WO_3)_2$ dimers at n = 16, all the way to a quantum supralattice of coupled $\{(WO_3)_2\}_2$ or $(WO_3)_4$ units at n = 32. With the data available in the loading range $16 < n \leq 32$, it did not prove possible to differentiate between the dimer-of-dimers and tetramer α-cage encapsulation models for $n(WO_3)$–$Na_{56}Y$.[4,9] A kind of connectivity or percolation threshold appears to occur around $n \simeq 8$ as was signaled by a red shift on the absorption edge of $n(WO_3)$–$Na_{56}Y$ and provides some evidence for intercavity (α-cage) electronic coupling between $(WO_3)_2$ dimer units.[4]

Evidence for local field effects arising from the presence of "half-naked" Na^+ supercage cations (or protons for $H_{56}Y$) interacting with the oxygen end of the carbonyl ligands of the precursor $W(CO)_6$ and located at the "surface" of the product $(WO_3)_2$ dimer has been found in the observation of $W(CO)_6$ and $(WO_3)_2$ induced alterations in the frequencies of mid-IR ZOH_α stretching modes and far-IR Na^+ translatory modes, ^{13}C, ^{29}Si, and ^{23}Na MAS-NMR chemical shifts, and $W_{4f,4d}$ XPS ionization potentials.[4,9] By intentionally varying the ionic potential of the constituent supercage cations in the series $16(WO_3)$–$M_{56}Y$, where M = H, Li, Na, K, Rb, Cs, it has proven possible to "fine tune" the band-gap of the tungsten(VI) oxide quantum supralattice by as much as 0.75 eV.[10]

In what follows we report EXAFS structure determinations for some key materials in the above story, namely, the precursor $8\{W(CO)_6\}$–$Na_{56}Y$ and photooxidation products $16(WO_3)$–$Na_{56}Y$ and $28(WO_3)$–$Na_{56}Y$.

Experimental Section

The precursor sample denoted $8\{W(CO)_6\}$–$Na_{56}Y$ and first and third stage photooxidation products (see above sequential saturation loading/photooxidation scheme) denoted $16(WO_3)$–$Na_{56}Y$ and $28(WO_3)$–$Na_{56}Y$ were prepared according to the procedures described previously.[4,8,9]

Data acquisition was carried out at the National Synchrotron Light Source at Brookhaven National Laboratories with a stored electron energy of 2.5 GeV and ring currents between 90 and 170 mA. The WL_{III} edge (10 207 eV) X-ray absorption data were collected on beamline X-11A and X-19A with a Si(111) crystal pair monochromator.

Measurements were performed in transmission at liquid nitrogen temperature. EXAFS samples were prepared such as to give a total absorption of about μx = 2.0 (μ = absorption coefficient, x = sample thickness) and an absorption step of about 1.0 at the edge to obtain an optimal signal-to-noise ratio. Zeolite powder was embedded in an octadecane/eicosane mixture and kept under a nitrogen atmosphere until data collection. Air stable compounds were finely ground and mixed with BN to give a self-supporting pellet.

The EXAFS data were analyzed following standard procedures[11] using a software package provided by D. C. Koningsberger. Background removal was accomplished by applying a Victoreen fit to the preedge region and a cubic spline function to the EXAFS data, the latter being fine-tuned by a smoothing parameter. Normalization to a per atom basis was performed by dividing the

(9) Ozin, G. A.; Özkar, S.; MacDonald, P. *J. Phys. Chem.* **1990**, *94*, 6939.
(10) Ozin, G. A.; Özkar, S.; Macdonald, P. M.; Moller, K.; Bein, T. Materials Research Society Proceedings, Anaheim, CA, May 1991.

(11) Lee, P. A.; Citrin, P. H.; Eisenberger, P.; Kincaid, B. M. *Rev. Mod. Phys.* **1981**, *53*, 769.

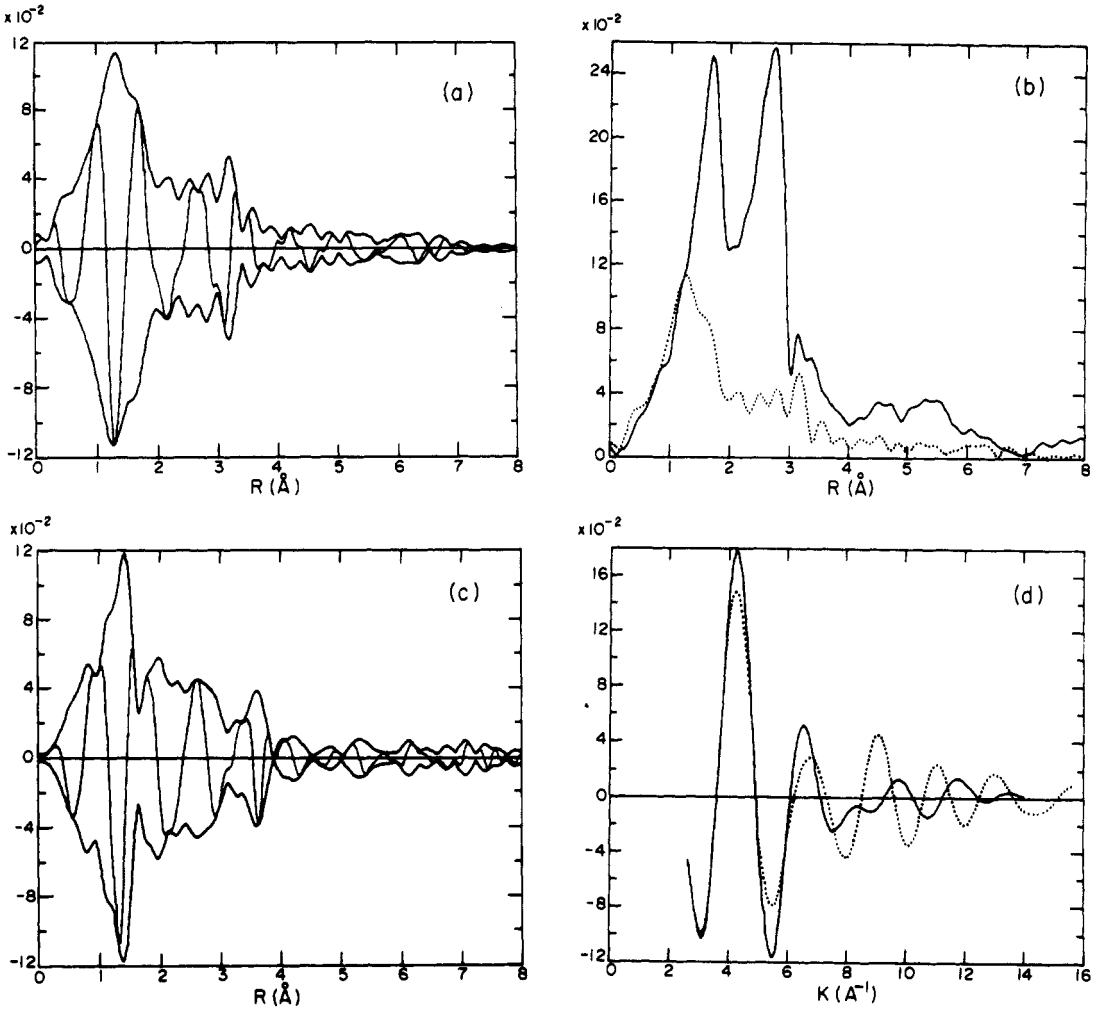

Figure 2. (a) k^1-weighed Fourier transformation (k = 3–14 Å^{-1}) of a sample 8{W(CO)$_6$}–Na$_{56}$Y, (b) overlay of magnitudes of Fourier transformations of sample 8{W(CO)$_6$}–Na$_{56}$Y (solid line) and 16(WO$_3$)–Na$_{56}$Y, (c) WO$_3$, and (d) overlay of the back-transformed first shell (0.0–1.9 Å) of sample 16(WO$_3$)–Na$_{56}$Y (solid line) and WO$_3$ (broken line).

TABLE I: Crystallographic Data of Reference Compounds

reference	atom pair	R/Å	N	ref
W(CO)$_6$	W–C	2.058	6	13
	W–CO	3.206	6	
Na$_2$WO$_4$	W–O	1.819	4	14
ReO$_2$	Re–Re	2.61	1	*a*
W powder	W–W	2.737	8	*b*
	W–W	3.258	6	
WO$_3$	W–O	1.7–2.2	6	*c*

[a] Magneli, A. *Acta Crystallogr.* **1956**, *9*, 1038. [b] *Strukturbericht*; 1937; Vol. 3, p 181. [c] Diehl, R.; Brandt, G.; Salje, E. *Acta Crystallogr.* **1978**, *B34*, 1111.

EXAFS spectrum by the height of the absorption edge which is proportional to the total number of absorbing atoms. The fitting procedure is based upon the plane-wave approximation using a least-squares routine. Phase functions and backscattering amplitudes used in the fitting procedure were extracted from reference compounds (Table I).

Results

Precursor Sample: 8{W(CO)$_6$}–Na$_{56}$Y. Hexacarbonyltungsten(0) adsorbed from the vapor phase into vacuum thermally dehydrated zeolite Na$_{56}$Y served as the precursor for the photooxidative synthesis of tungsten oxide clusters.[4,8,9] EXAFS measurements were performed with a sample loaded with eight W(CO)$_6$ molecules per unit cell (that is, one W(CO)$_6$ per α-cage), denoted 8{W(CO)$_6$}–Na$_{56}$Y, as well as on neat W(CO)$_6$. After background subtraction and normalization, a Fourier transformation was applied to the data, weighed by k^1, resulting in a radial distribution function of atoms surrounding the tungsten absorber. Spectra for (a) W(CO)$_6$ and (b) 8{W(CO)$_6$}–Na$_{56}$Y are shown in Figure 1. At this stage of the analysis, peak positions give only approximate bond distances, due to an element-specific phase shift. Accurate values are obtained by fitting with adequate reference compounds.

A qualitative comparison between parts a and b of Figure 1 immediately reveals a strong similarity between pure W(CO)$_6$ and that same compound adsorbed in the zeolite. A fit was performed separately on the W–C and W–CO ligand sphere on sample 8 {W(CO)$_6$}–Na$_{56}$Y with the reference W(CO)$_6$. The back-transformed individual carbon and oxygen shells are shown in Figure 1c,d where they are overlayed with the fitting result. The resulting coordination numbers of 6.5 and 6.8 and bond distances of 2.06 and 3.21 Å, respectively, are within the limits of accuracy, identical with the reference compound W(CO)$_6$ (see Tables I and II).

First Stage Saturation Loading/Photooxidation Product: 16(WO$_3$)–Na$_{56}$Y. A Fourier transformation similar to the precursor 8{W(CO)$_6$}–Na$_{56}$Y was performed on the photooxidation product 16(WO$_3$)–Na$_{56}$Y and is shown in Figure 2a. The latter was synthesized by $\lambda > 240$ nm xenon lamp, room-temperature photolysis of 16{W(CO)$_6$}–Na$_{56}$Y using 400 Torr of dry O$_2$.[4,9] The dramatic structural changes that have occurred on oxidation are best visible in Figure 2b, where the magnitudes of the Fourier transformation of precursor sample 8{W(CO)$_6$}–Na$_{56}$Y and product sample 16(WO$_3$)–Na$_{56}$Y are overlayed. A strong reduction in the W–C and W–CO coordination signals the loss of the carbonyl ligands. Simultaneously, a new peak at much shorter distances is visible at about 1.3 Å (uncorrected for phase shift). As the intrazeolite photoproduct has been shown to be tung-

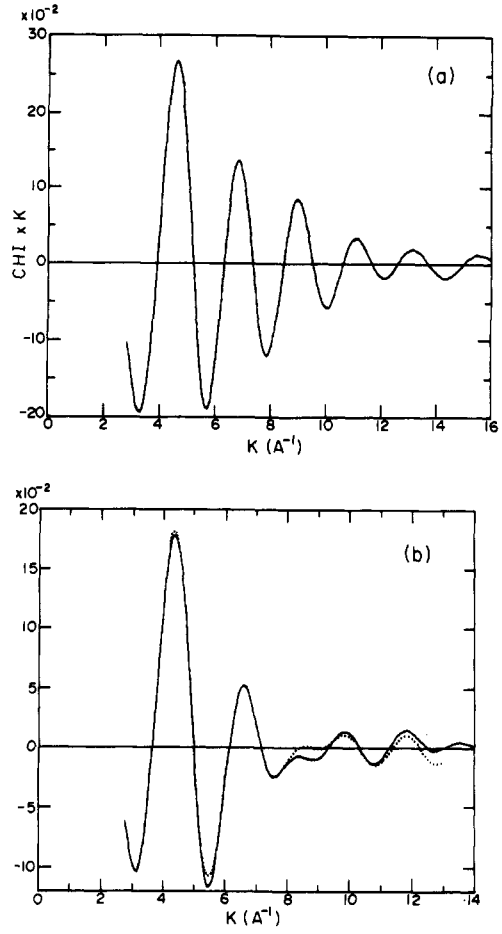

Figure 3. (a) Back-transformed first shell (0.0–1.9 Å) of reference Na_2WO_4 and (b) of sample $16(WO_3)$–$Na_{56}Y$ (solid line), overlayed with fit results (broken line).

sten(VI) oxide,[4,9] the bulk monoclinic form of WO_3 was also measured for qualitative comparison and is shown in Figure 2c. The first shells (0–2 Å) of bulk WO_3 and sample $16(WO_3)$–$Na_{56}Y$ are somewhat comparable, but the back-transformation of these contributions clearly shows a different ligand distribution in both compounds (see Figure 2d). WO_3 shows a strong damping of the second modulation in its EXAFS spectrum (broken line), while $16(WO_3)$–$Na_{56}Y$ has a distinctive node at $k = 8$ Å^{-1} (solid line) which may be attributed to the presence of two closely spaced ligand shells. (Monoclinic WO_3 has a broad distribution of W–O bond lengths between 1.71 and 2.21 Å).

Fitting of sample $16(WO_3)$–$Na_{56}Y$ was performed with sodium tungstate as a reference compound. The back-transformed oxygen coordination of Na_2WO_4 is shown in Figure 3a. The smooth decay of the oscillation is characteristic for the presence of only one bond distance to the absorber atom. In contrast, the complex amplitude function of sample $16(WO_3)$–$Na_{56}Y$ when back-transformed indicates more than one nearest-neighbor distance in the first shell (Figure 3b). When $16(WO_3)$–$Na_{56}Y$ was analyzed by using a two-shell fit, which accounts for two different tungsten–oxygen distances, a stable solution was obtained with a W–O bond at 1.77 Å and a coordination number of 2.2 and a second W–O bond at 1.94 Å with a coordination number of 1.8. The final result is seen in Figure 3b, where the original data (solid line) are overlayed with the fit (broken line). Comparison with crystallographic data of molybdenum(VI) or tungsten(VI) oxides shows that terminal metal–oxygen double bonds have bond lengths of ca. 1.7 Å, while doubly and triply bridged metal–oxygen bonds appear at ca. 1.9 and 2.3 Å, respectively.[12] Hence, the fit result of 1.94 Å points to the presence of support-coordinated or multinuclear tungsten(VI) oxide clusters.

(12) Day, V. W.; Klemperer, W. G. *Science* **1985**, *228*, 533.

TABLE II: Structural Data As Derived from EXAFS Analysis

sample	atom pair	N^a	R/Å^b	$\Delta\sigma^2$/Å^{2c}	ΔE/eV^d
$8\{W(CO)_6\}$–$Na_{56}Y$	W–CO	6.5	2.06	0.0003	0.7
	W–CO	6.8	3.21	0.0003	−0.5
$16(WO_3)$–$Na_{56}Y$	W–O	2.2	1.77	0.0008	3.8
	W–O	1.8	1.94	−0.0009	3.8
	W–W	1.3	3.30	0.0009	−6.9
$28(WO_3)$–$Na_{56}Y$	W–O	2.2	1.75	0.0030	3.6
	W–O	2.2	1.95	0.0010	−3.9
	W–W	1.4	3.24	0.0016	4.3

[a] Coordination number. [b] Bond distance. [c] Static disorder. [d] Inner potential.

As observed in Figure 2a, a smaller contribution at ca. 3.1 Å occurs in the Fourier transformation. This peak is again different to that in bulk WO_3, which has several W–W distances at ca. 3.7 Å. To evaluate this contribution, a k^3-weighed Fourier transformation was applied to sample $16(WO_3)$–$Na_{56}Y$, which will enhance the magnitude of scattering when heavy backscatterers are present. The resulting spectrum is shown in Figure 4b. Clearly, the peak at 3.1 Å has grown in intensity and is accompanied by side lobes (compare to Figure 2a). The signature of back-transformed peaks from the real space data is indicative for the nature of the respective ligand, and a number of such transformations with different windows were applied to this outer contribution. An example is shown in Figure 4d. The observed second maximum at $k = 12$ Å^{-1} in the EXAFS modulation is a *strong indication for the presence of a heavy scatterer, such as tungsten.* Other elements present in this sample like sodium or silicon cannot be responsible for this maximum at ca. 12 Å^{-1} since their amplitude functions fall off rapidly at higher k values. However, they do seem to be convoluted in this peak, giving rise to the strong contribution between 2 and 6 Å^{-1}. The data analysis of this complex function was approached by fitting only the range between 6 and 14 Å^{-1} in Figure 4-d, thereby discriminating any influence of light elements. Assuming that a W–O–W scatterer pair is predominant in this range, an adequate reference had to be found. The strong disorder in the second shell of WO_3 excludes this oxide as a candidate, and the Re–O–Re shell of ReO_2 was chosen instead. Its Fourier transformation and back-transformation are shown in Figure 4a,c. A fit performed with this reference resulted in a W···W bond length of 3.30 Å and a W···W coordination number of 1.3 (see Table II). Inclusion of other scatterer pairs in the fit, e.g. W···Si atoms and W···Na, did not give unique fit solutions. (Large static disorder was always observed). However, the presence of a W···W scatterer pair could clearly be established. The obtained bond length of 3.30 Å suggests a bent rather than a linear W–O–W structure. Doubly oxygen bridged tungsten(VI) centers have a bond distance of ca. 3.3 Å, while singly oxygen bridged ones are ca. 3.7 Å apart.[12]

Third Stage Sequential Saturation Loading/Photooxidation Product: $28(WO_3)$–$Na_{56}Y$. The EXAFS data set and analysis results for the title sample proved to be remarkably similar to that described above for the first stage saturation loading/photooxidation product $16(WO_3)$–$Na_{56}Y$ (Table II). Using a similar fitting procedure for $28(WO_3)$–$Na_{56}Y$ as used for $16(WO_3)$–$Na_{56}Y$, one again finds the presence of two different tungsten–oxygen distances, with a stable solution having a W–O bond at 1.75 Å and a coordination number of 2.2 and a second W–O bond of 1.96 Å with a coordination number of 2.2. The existence of a W···W scatterer pair was also clearly defined with a bond length of 3.24 Å and a W···W coordination number of 1.4 (see Table II). From these results it would therefore appear that the sequential addition of WO_3 units to the $16(WO_3)$–$Na_{56}Y$ sample simply enhances the $(WO_3)_2$ dimer population. In view of the fact that $16(WO_3)$–$Na_{56}Y$ already contains one $(WO_3)_2$ dimer moiety per α-cage, the further addition of WO_3 units is envisaged as a continued buildup of α-cage $(WO_3)_2$ dimers, resulting in an accumulation of α-cage encapsulated dimers-of-dimers $\{(WO_3)_2\}_2$ rather than α-cage cluster growth to trimers $(WO_3)_3$ and/or tetramers $(WO_3)_4$. The geometric and spatial feasibility of the favored α-cage dimer-of-dimers $\{(WO_3)_2\}_2$ aggregate can be as-

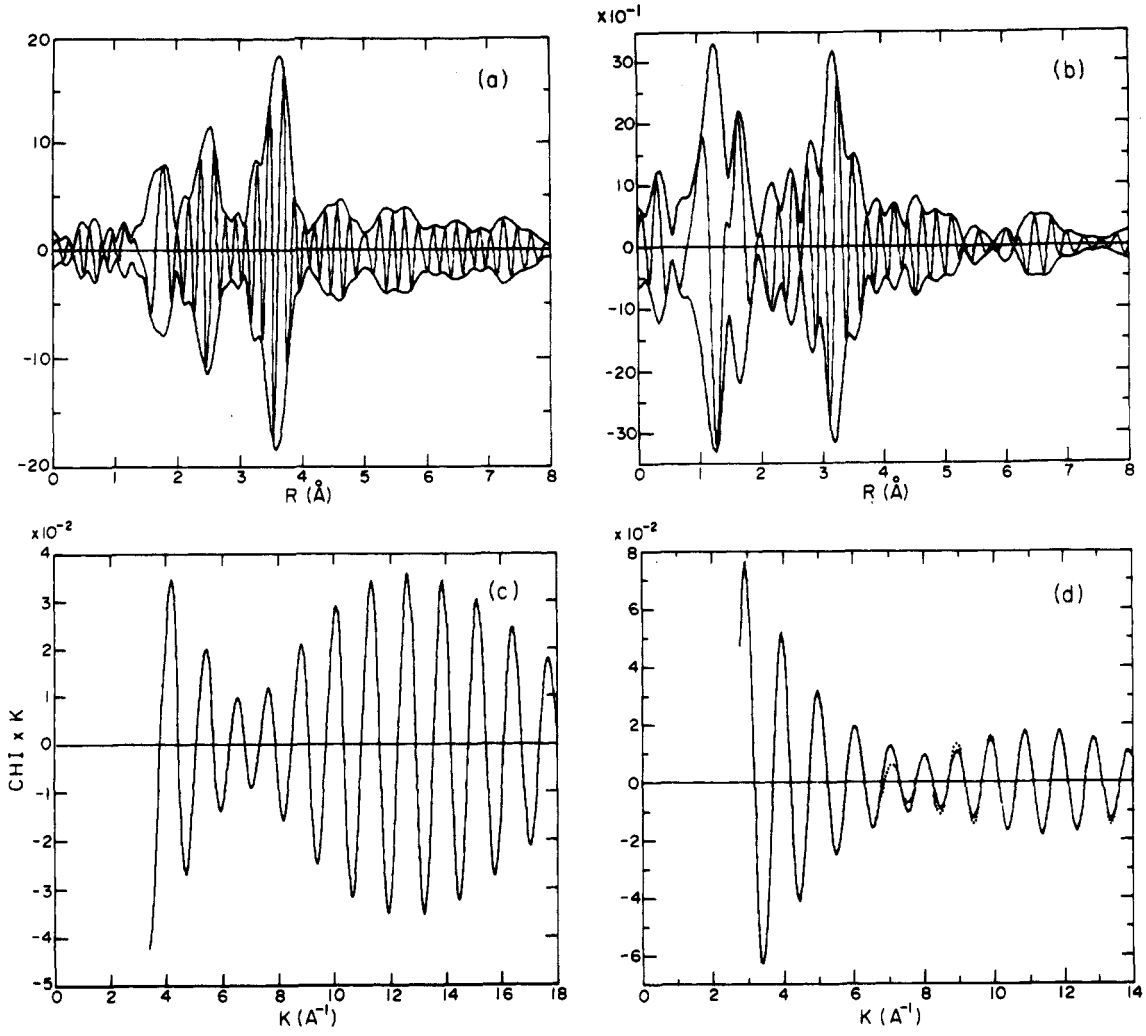

Figure 4. k^3-weighed Fourier transformation of (a) reference ReO_2 (k = 3.5–18 Å^{-1}) and (b) of sample 16(WO_3)–$Na_{56}Y$ (k = 2.8–14 Å^{-1}). (c) Back-transformed Re–Re atom pair of ReO_2 (2.2–2.7 Å) and (d) back-transformed outer shell of sample 16(WO_3)–$Na_{56}Y$ (2.7–3.5 Å, solid line) and fit (broken line).

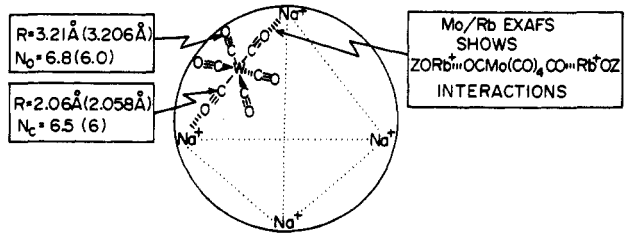

Figure 5. Summary illustration of the structural data for the precursor 8{$W(CO)_6$}–$Na_{56}Y$ and pure $W(CO)_6$ as derived from EXAFS. N_O is the coordination number for W–CO, N_C is the coordination number for W–CO, and numbers in parentheses are structural data for the precursor, $W(CO)_6$.

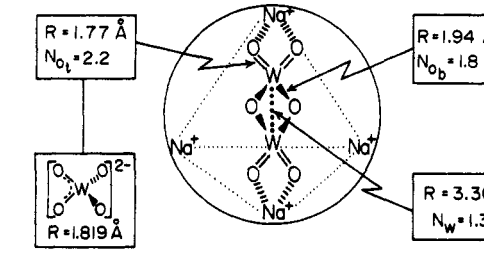

Figure 6. Summary illustration of the structural data for the photooxidation product 16(WO_3)–$Na_{56}Y$ as derived from EXAFS. N_{Ot} is the coordination number for terminal W=O, N_{Ob} is the coordination number for bridging W···O, and N_W is the coordination number for W···W.

certained from a CHEM-X molecular graphics structural model for two orthogonally configured, α-cage immobilized ZONa···O_2W-(μ-O)$_2$$WO_2$···NaOZ moieties, involving adjacent Na^+ site II cation six-ring anchoring sites (Figure 7).

Conclusions

The structural data for the precursor 8{$W(CO)_6$}–$Na_{56}Y$ and photooxidation products 16(WO_3)–$Na_{56}Y$ and 28(WO_3)–$Na_{56}Y$ as derived from the present EXAFS study, when taken in combination with earlier chemical and spectroscopic information from these laboratories for related systems,[4,8,9] allow one to arrive at the conclusions illustrated in Figures 5–7. The central points to emerge from this study are summarized below.

(i) $W(CO)_6$ maintains its structural integrity when housed in the α-cage of $Na_{56}Y$ with only minor perturbations of the skeletal WC and ligand CO bonds compared to those found for the free molecule (Figure 5).[13] Similar results have recently been found for 8{$Mo(CO)_6$}–$Rb_{56}Y$, where evidence for the interaction of the $Mo(CO)_6$ guest with extraframework Rb^+ cations was determined by a combination of molybdenum and rubidium edge EXAFS data[8] (Figure 5).

(ii) In the case of 16(WO_3)–$Na_{56}Y$, the presence of two terminal oxygens (1.77 Å) and two bridging oxygens (1.94 Å) per tungsten, together with a short distance to a second tungsten (3.30

(13) Arnesen, S. P.; Seip, H. M. *Acta Chem. Scand.* **1966**, *20*, 2711.
(14) Okada, K.; Morikawa, H.; Marumo, F.; Iwai, S. *Acta Crystallogr.* **1974**, *B30*, 1872.

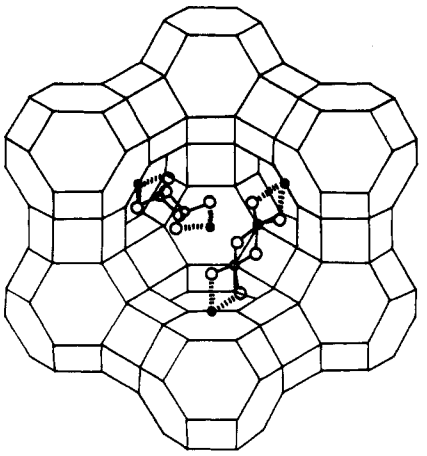

Figure 7. CHEM-X model for two orthogonally oriented, α-cage immobilized $ZONa\cdots O_2W(\mu\text{-}O)_2WO_2\cdots NaOZ$ moieties, involving adjacent Na^+ site II cation six-ring anchoring sites.

Å), suggests that the EXAFS data are best explained in terms of the formation of a tungsten(VI) oxide dimer $(WO_3)_2$ (Figure 6), occupying every α-cage of $Na_{56}Y$.

(iii) The $(WO_3)_2$ molecular dimer unit displays terminal tungsten–dioxo bond lengths of 1.77 Å, which falls in a range intermediate between those having formal bond orders of 2 (e.g. 1.69–1.70 Å in $W_6O_{19}^{2-}$)[12] and $1^1/_2$ (e.g. 1.82 Å in WO_4^{2-}).[10] This observation provides indirect evidence for the interaction of the terminal tungsten–dioxo groups of the $(WO_3)_2$ guest with extraframework Na^+ cations as illustrated in Figure 6, a deduction which is in line with the conclusions drawn from earlier chemical and spectroscopic measurements on similar systems.[4,8,9] The tungsten–oxygen bond length of 1.94 Å found for the bridging $W(\mu\text{-}O)_2W$ unit of the dimer falls in the range expected for doubly oxygen bridged tungsten(VI), e.g., 1.92 Å found in $W_6O_{19}^{2-}$.[12]

(iv) The dimer structural unit illustrated in Figure 6 is fully consistent with the EXAFS derived tungsten–oxygen and tungsten–tungsten bond lengths and coordination numbers (Table II).

(v) The sequential addition of WO_3 units to the $16(WO_3)$–$Na_{56}Y$ quantum supralattice composed of $(WO_3)_2$ dimers is visualized as a continued buildup of α-cage $(WO_3)_2$ dimers, resulting in an accumulation of α-cage encapsulated dimers-of-dimers $\{(WO_3)_2\}_2$ (Figure 7) rather than cluster accretion to α-cage trimers $(WO_3)_3$ and/or tetramers $(WO_3)_4$.

Acknowledgment. We acknowledge the Natural Sciences and Engineering Research Council of Canada's Operating and Strategic Grants Programmes for generous financial support of this work. S.O. expresses his gratitude to the Middle East Technical University for granting him an extended leave of absence to conduct his research at the University of Toronto. K.M. and T.B. acknowledge partial funding for this work from the donors of the Petroleum Research Fund, administered by the American Chemical Society. The operational funds for NSLS beamline X-11A are provided by DOE Grant DEAS0580ER10742. Supplies of high-quality zeolites from Dr. Edith Flanigen at Union Carbide, Tarrytown, NY, are gratefully appreciated.

Registry No. $W(CO)_6$, 14040-11-0; WO_3, 1314-35-8.

Low-Frequency Single-Crystal Raman, Far-Infrared, and Inelastic Neutron Scattering Studies of Acetanilide at Low Temperature

Clifford T. Johnston,*

Department of Soil Science, University of Florida, Gainesville, Florida 32611

Stephen F. Agnew,† Juergen Eckert,‡ Llewellyn H. Jones,† Basil I. Swanson,† and Clifford J. Unkefer†

INC-4 and P-LANSCE, Los Alamos National Laboratory, Los Alamos, New Mexico 87545
(Received: May 11, 1990; In Final Form: January 22, 1991)

Single-crystal Raman, far-infrared (far-IR), and inelastic neutron scattering (INS) spectra of acetanilide (ACN) in the low-frequency region (20–200 cm^{-1}) were obtained as a function of temperature. At 20 K, a total of 29 low-frequency Raman-active vibrational modes were resolved and assigned to a unique symmetry species. For comparison, a total of 23 far-IR bands were observed in the 20–200-cm^{-1} region at 20 K. Factor group analysis of ACN predicts 24 Raman-active and 15 IR-active phonon bands. The greater-than-expected number of observed bands in the low-frequency region was assigned to the presence of low-frequency internal modes that exhibit anomalous frequency-shift and line-narrowing behavior upon cooling. The most striking change occurs in the B_{1g} (xy) polarization where a single band at 126 cm^{-1} at 305 K splits into three distinct, well-resolved bands at 133, 142, and 152 cm^{-1} at 20 K. INS spectra of ACN and its deuterated isotopomers demonstrate clearly that the 142-cm^{-1} band corresponds to a methyl torsion. In addition, low-frequency bands at 104 and 189 cm^{-1} were assigned to internal modes. In contrast to the phonon modes, the low-frequency internal modes all exhibit greater line broadening with temperature.

Introduction

The anomalous temperature dependence of the amide-I region of crystalline acetanilide (ACN) has received considerable attention recently.[1-13,26] In the amide-I region, crystalline ACN is characterized by two strong Raman-active amide-I bands at 1665 cm^{-1} (A_g) and 1678 cm^{-1} (B_{1g}), and one IR-active band at 1665 cm^{-1} at 300 K. When ACN is cooled, a new IR- and Raman-active band appears at 1650 cm^{-1}, which increases in

† INC-4.
‡ P-LANSCE.

(1) Sauvajol, J. L.; Almairac, R.; Moret, J.; Barthes, M.; Ribet, J. L. *J. Raman Spectrosc.* **1989**, *20*, 517.
(2) Blanchet, G. B.; Fincher, C. R., Jr. *Phys. Rev. Lett.* **1985**, *54* (12), 1310.
(3) Scott, A. C.; Bigio, I. J.; Johnston, C. T. *Phys. Rev. B* **1989**, *39*, 12883.
(4) Johnston, C. T.; Swanson, B. I. *Chem. Phys. Lett.* **1985**, *114* (5, 6), 547.

0022-3654/91/2095-5281$02.50/0